

Supporting Information

Lithiated Polymer Coating for Interface Stabilization in Li₆PS₅Cl-Based Solid-State Batteries with High-Nickel NCM

Bing-Xuan Shi,^a Franjo Weber,^b Yuriy Yusim,^a Thomas Demuth,^c Kilian Vettori,^a Andreas Münchinger,^d Giorgi Titvinidze,^{d,e} Kerstin Volz,^c Anja Henss,^a Rüdiger Berger,^b Felix H. Richter^{*a}

^a Institute of Physical Chemistry & Center for Materials Research (LaMa), Justus-Liebig-University Giessen, Heinrich-Buff-Ring 17, 35392 Giessen, Germany

^b Max Planck Institute for Polymer Research, Ackermannweg 10, 55128, Mainz, Germany.

^c Department of Physics & Materials Sciences Center (WZMW), Philipps-University Marburg, Hans-Meerwein Straße 6, 35032 Marburg, Germany.

^d Hahn-Schickard, Georges-Köhler-Allee 103, 79110 Freiburg, Germany

^e Agricultural University of Georgia, 240 David Aghmashenebeli Alley, 0131 Tbilisi, Georgia

* Corresponding author, Felix.H.Richter@phys.chemie.uni-giessen.de

Keywords: Solid-state batteries, polymer coating, cathode, solid electrolyte, interface degradation, polyanion

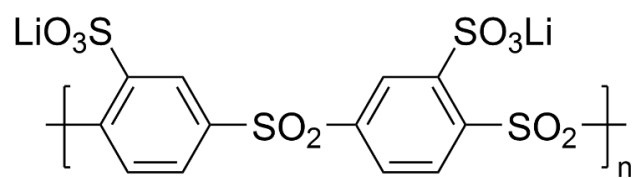


Figure S1. Chemical structure of sulfonated poly(phenylene sulfone) in its lithiated form (sPPSLi).

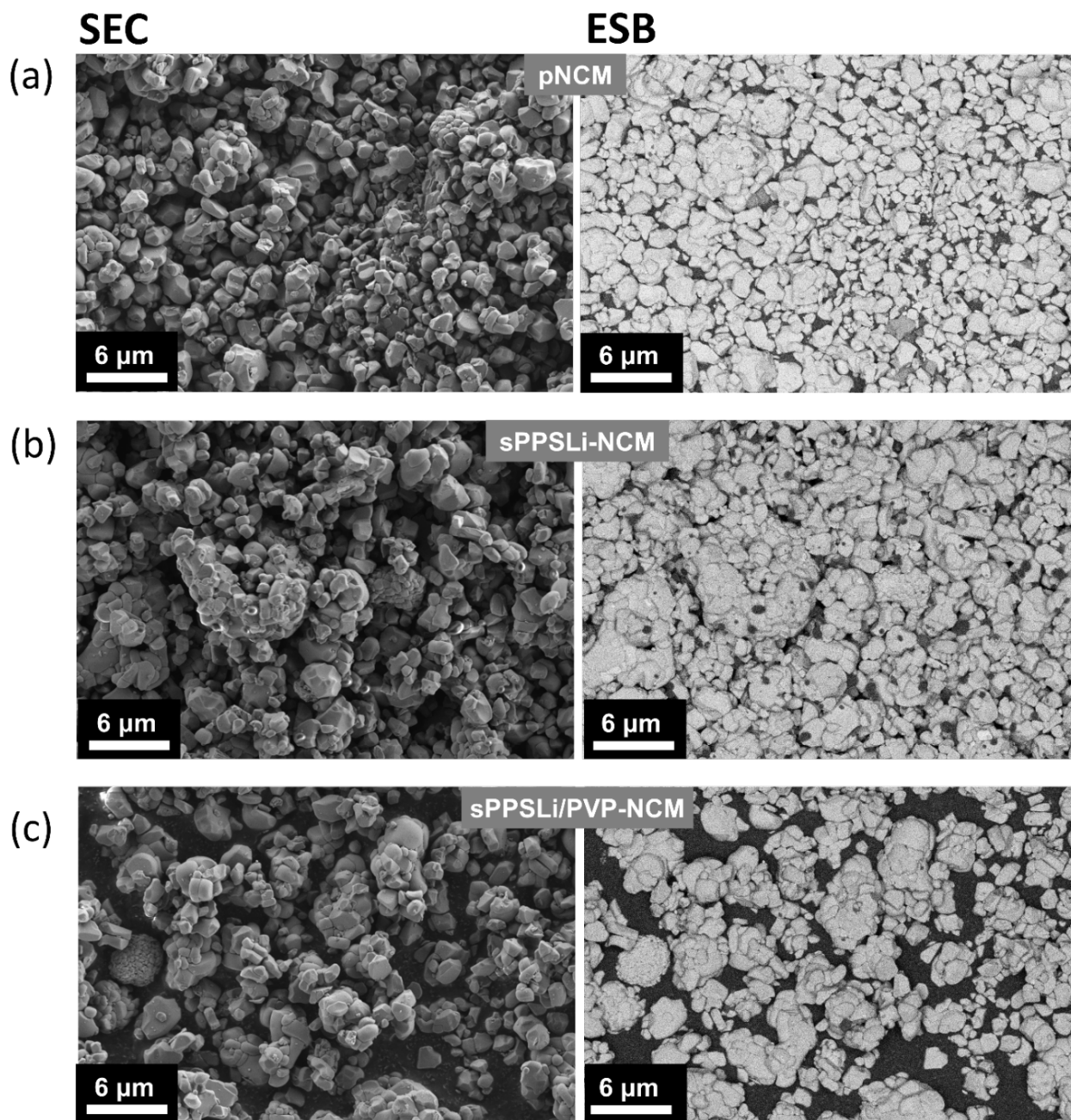


Figure S2. SEM analysis of (a) pNCM, (b) sPPSLi-NCM, and (c) sPPSLi/PVP-NCM with secondary electron images (SEC) shown on the left and energy-selective backscattered electron images (ESB) shown on the right. (Interpretation: sPPSLi-NCM shows some polymer particle aggregation on the surface of NCM, which is evident as dark spots visible in the ESB image of sPPSLi-NCM; in contrast, sPPSLi/PVP-NCM and pNCM show no polymer particles, suggesting that the sPPSLi/PVP-NCM is coated uniformly.)

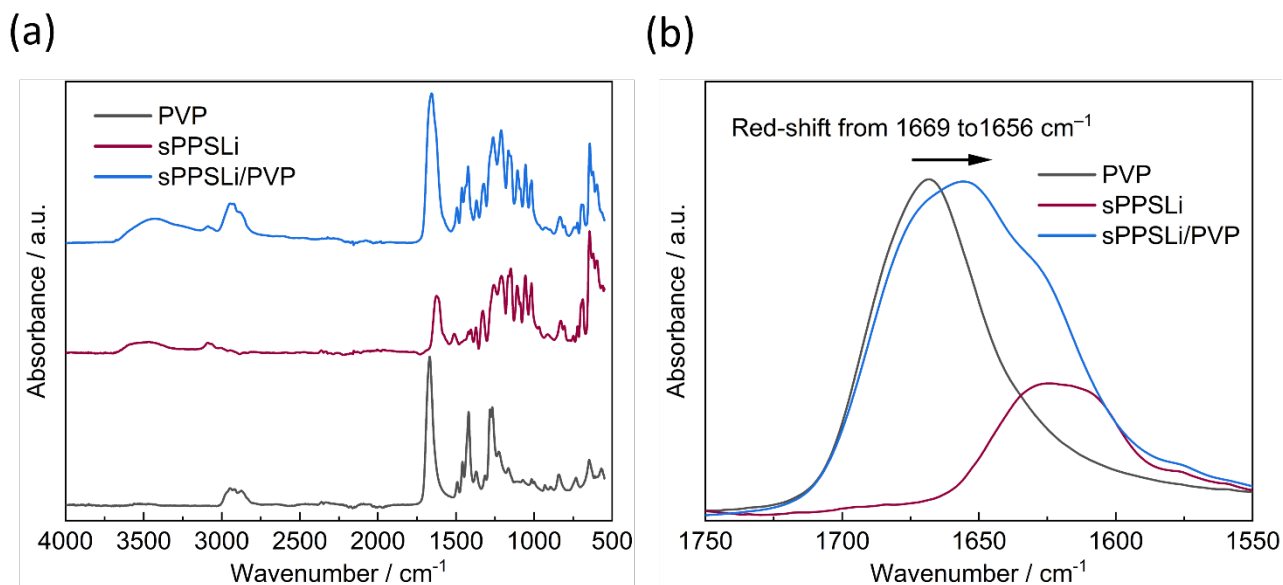


Figure S3. (a) FT-IR spectra of PVP, sPPSLi, and sPPSLi/PVP mixture with 1:1 weight ratio (96 scans each). (b) Magnification of the image in (a) to focus on the region with 1550 cm^{-1} to 1750 cm^{-1} wavenumber. (Interpretation: this region corresponds to the C=O bond. The electrostatic interaction between PVP and sPPSLi is evident from the red-shift observed in the C=O stretching frequency, moving from 1669 cm^{-1} to 1656 cm^{-1} .)

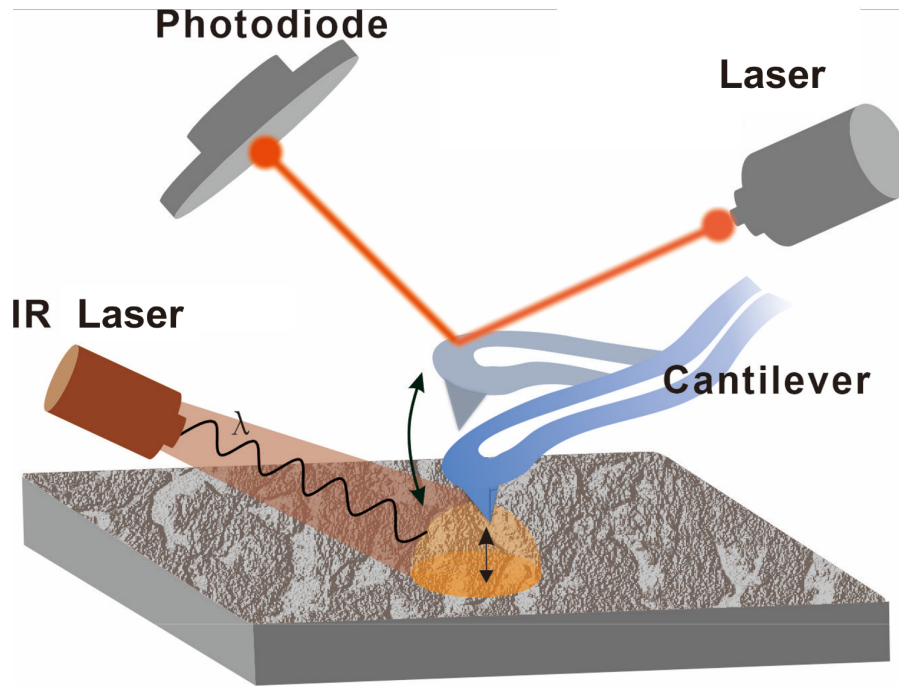


Figure S4. Schematic of the working principle of nano-infrared microscopy (nano-IR).

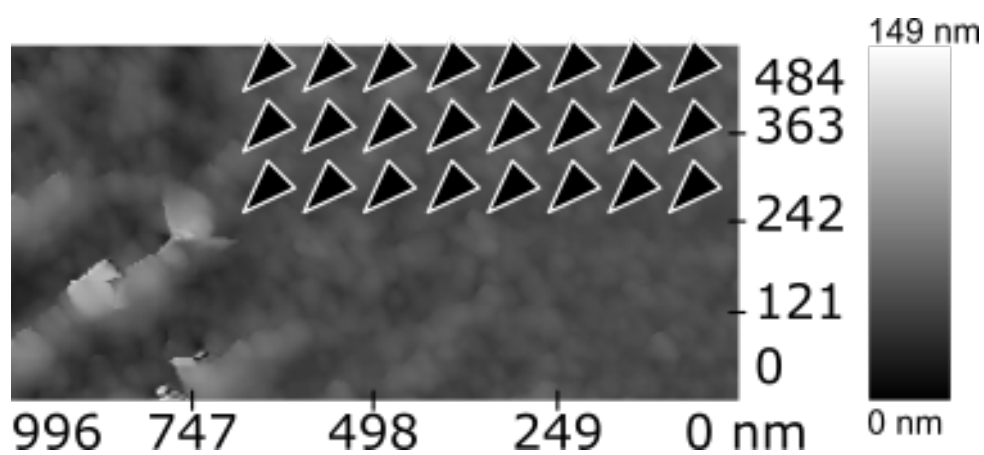


Figure S5. Topography of the sPPSLi/PVP polymer film with positions where photo-induced force microscopy was performed (black triangles). The sPPSLi/PVP polymer film is prepared by pressing sPPSLi/PVP powder into a pellet.

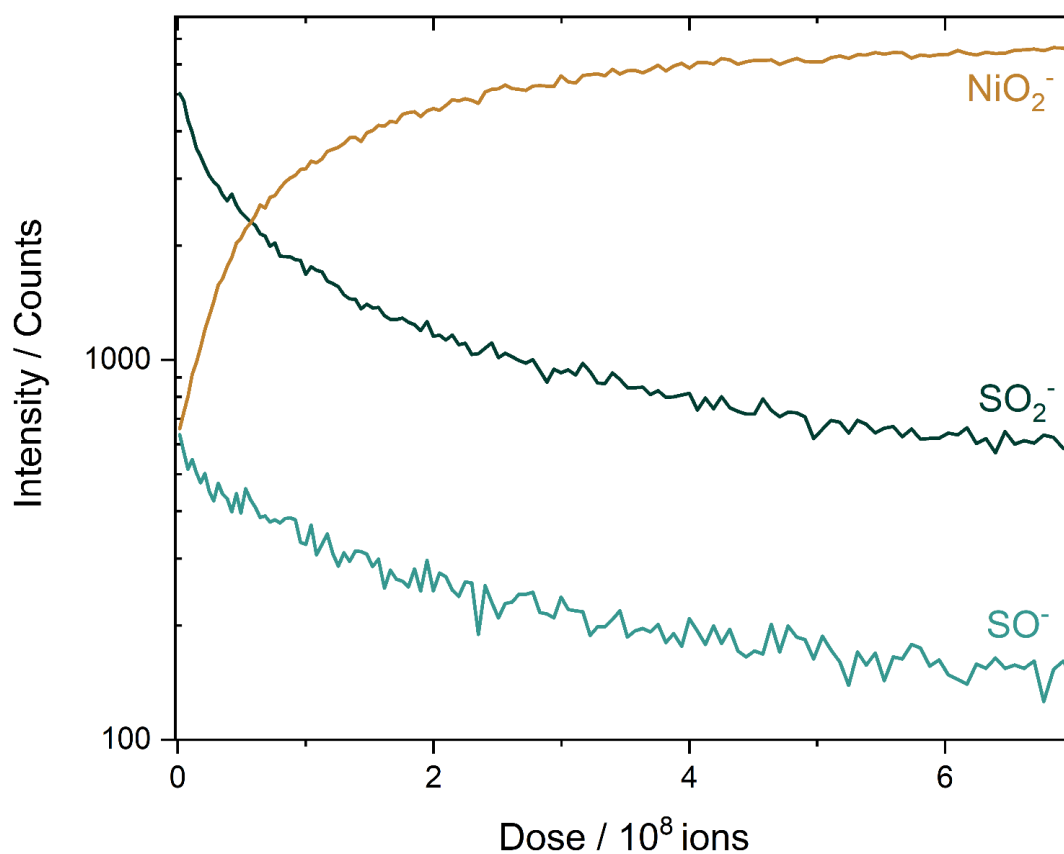


Figure S6. ToF-SIMS depth profiles of sPPSLi/PVP-NCM following the SO₂⁻, SO⁻, and NiO₂⁻ fragments. (Interpretation: the SO₂⁻ and SO⁻ signals decrease, and the NiO₂⁻ signal increases when analyzing the surface in the imaging mode with Bi³⁺ as primary ions (0.1 pA). This indicates that the polymer is gradually removed from the surface of the sPPSLi/PVP-NCM particles during the measurement.)

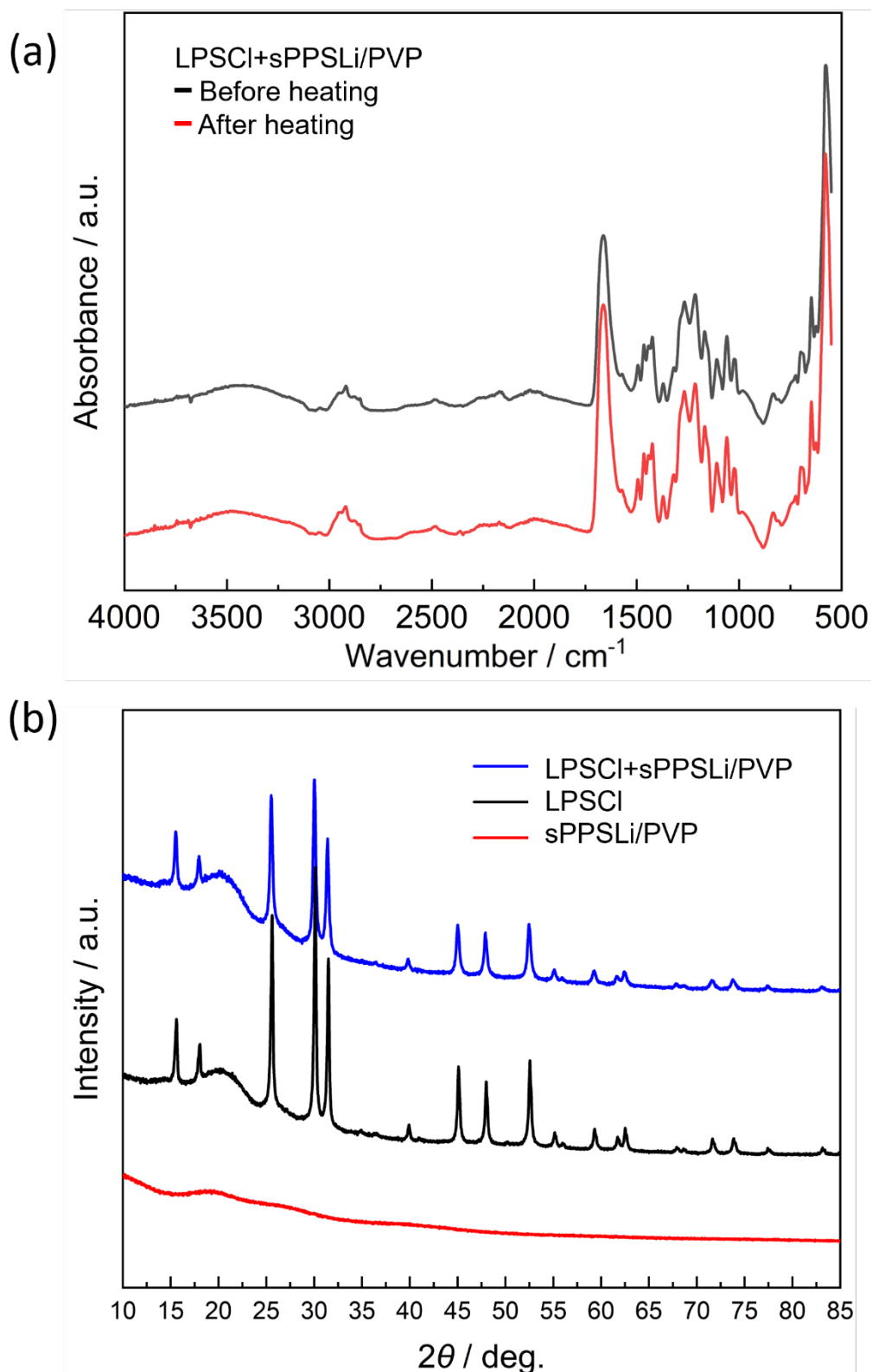


Figure S7. (a) FT-IR of $\text{Li}_6\text{PS}_5\text{Cl}$ mixed with sPPSLi/PVP polymer complex shows no difference before and after heating in a vacuum chamber at 80 °C for 24 hours. (b) XRD patterns of sPPSLi/PVP mixed with $\text{Li}_6\text{PS}_5\text{Cl}$ after heating at 80 °C for 24 hours also match the reflections of $\text{Li}_6\text{PS}_5\text{Cl}$ before heating. In addition, sPPSLi/PVP is shown to be amorphous.

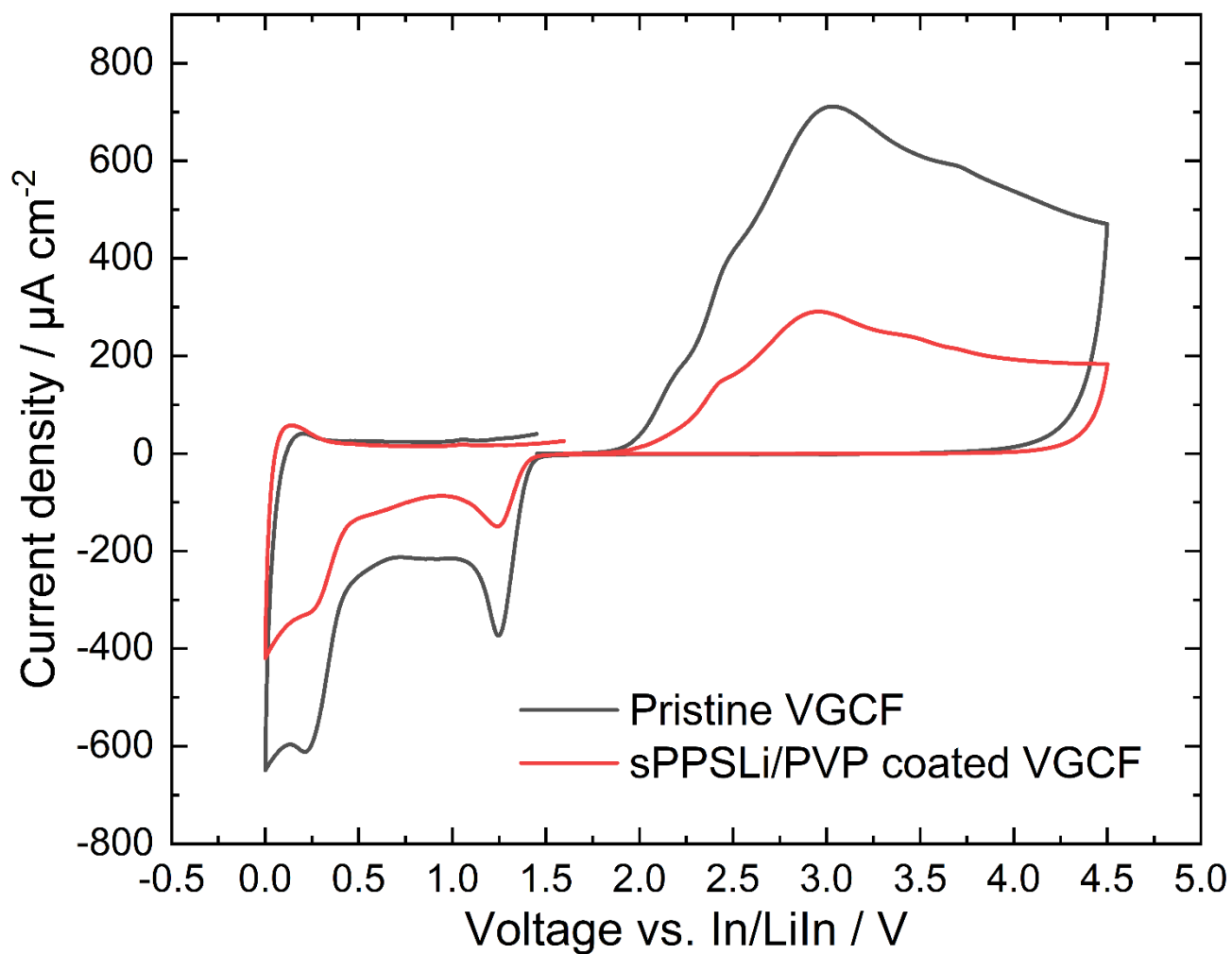


Figure S8. The electrochemical stability window is measured by cyclic voltammetry for the range of 0 V to 4.5 V (vs. In/LiIn) with a scan rate of 1 mV s^{-1} , initiating from the open circuit potential. The electrochemical cell was constructed using VGCF/ $\text{Li}_6\text{PS}_5\text{Cl}$ composite as the working electrode, $\text{Li}_6\text{PS}_5\text{Cl}$ as the separator, and an indium-lithium alloy as the counter electrode.

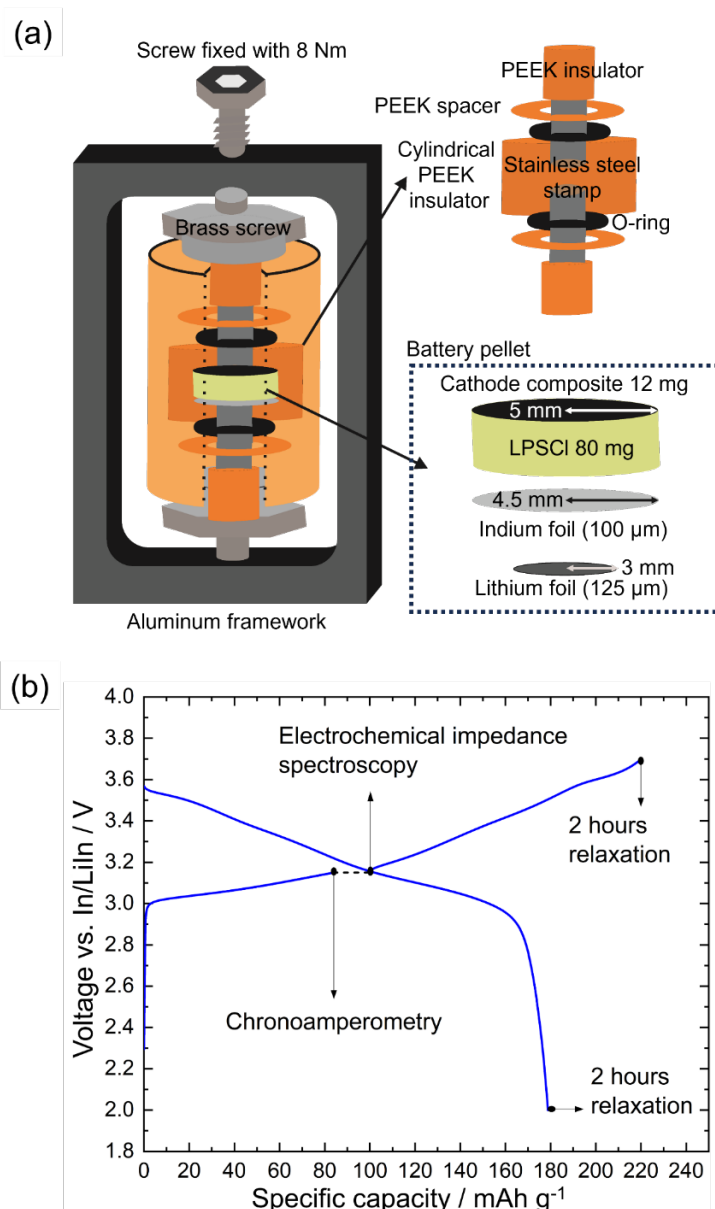


Figure S9. (a) Schematic illustrating the cell casing and the architecture of the SEB pellet. The SEB pellet comprises 12 mg of cathode composite, 80 mg of $\text{Li}_6\text{PS}_5\text{Cl}$ solid electrolyte separator, 9 mm in diameter of indium foil, and 6 mm in diameter of lithium foil, all compacted within a PEEK cylinder. Stainless steel terminals serve as current collectors, while O-rings ensure the SEB pellet remains airtight and protected from external air. (b) Schematic of performed electrochemical analysis. SEBs are initially galvanostatically charged to 3.15 V (vs. In/LiIn). They are held at this potential until the current decreases to below 2% (chronoamperometry). Following this, EIS measurements are taken from 1 MHz to 100 μHz . EIS sinusoidal amplitudes are set at 10 mV (from 1 MHz to 10 mHz), 5 mV (from 10 mHz to 1 mHz), and finally 3 mV (from 1 mHz to 100 μHz). The SEBs are then galvanostatically charged to 3.7 V (vs. In/LiIn), followed by a 2-hour relaxation period. Finally, they are discharged to 2.0 V (vs. In/LiIn) and then undergo another 2-hour relaxation period. The relaxation periods are required for the active mass calculation.

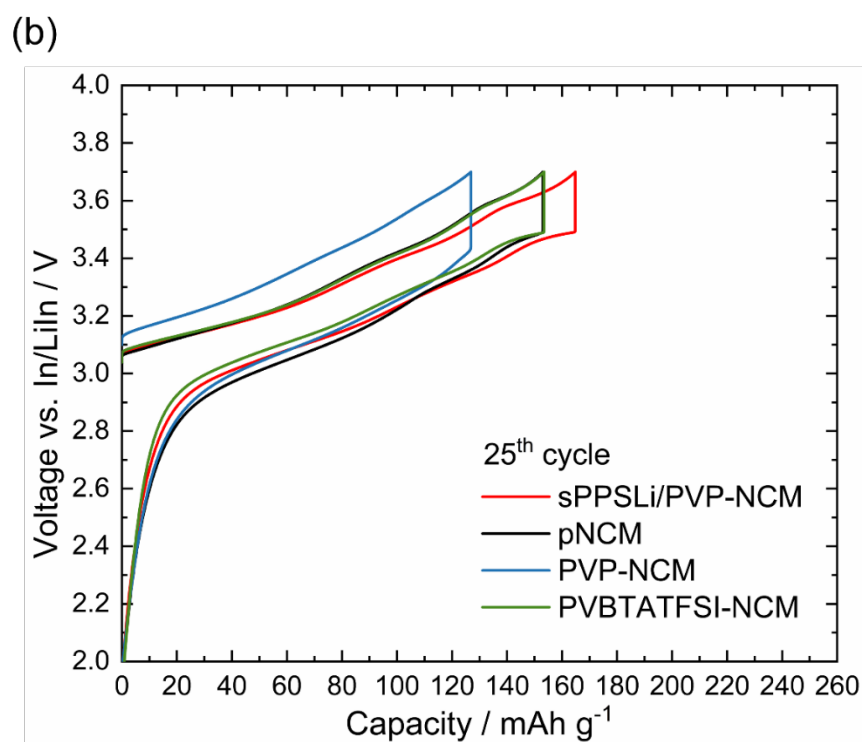
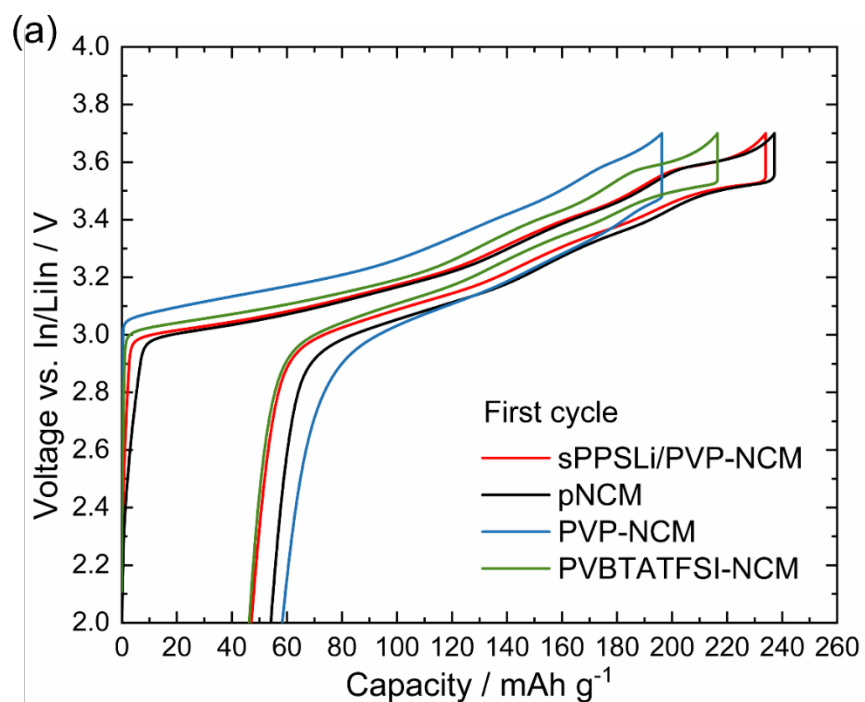


Figure S10. Charge/discharge curves of the (a) first and (b) 25th cycle at 0.1C.

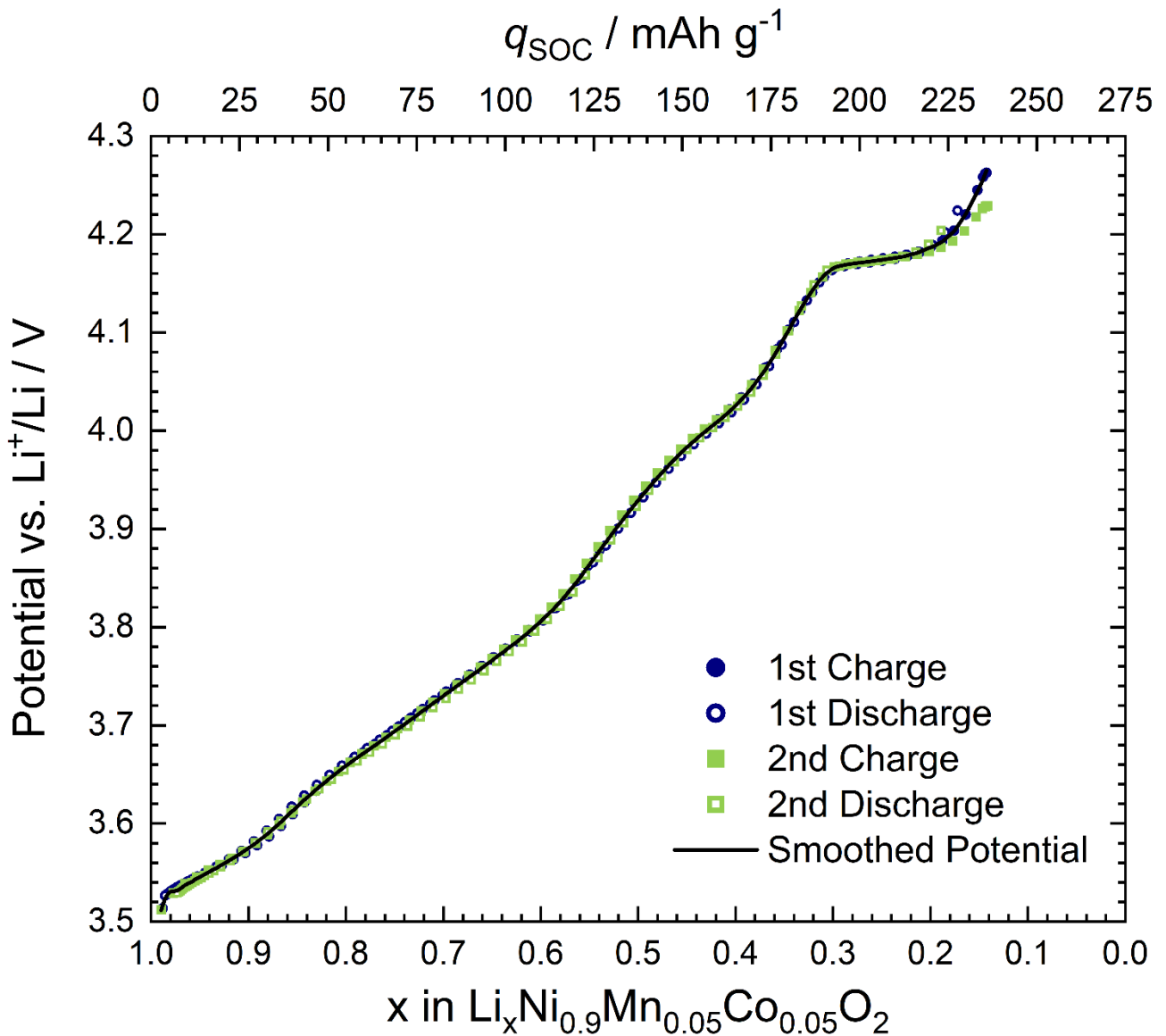


Figure S11. Illustration of the relationship between the open circuit voltage (OCV) (vertical axis) and the state of charge (SOC), represented by the Li^+ content x in $\text{Li}_x\text{Ni}_{0.9}\text{Mn}_{0.05}\text{Co}_{0.05}\text{O}_2$ (horizontal axis). This relationship is derived from galvanostatic charge-discharge cycles of a $\text{LiLEB}^{\text{NCM}}$ at a rate of 0.1C. Every 10-minute interval of charging or discharging is followed by a two-hour relaxation period to measure the OCV. Using the known time and current to obtain the amount of charge per GITT pulse step, we can calculate x in $\text{Li}_x\text{Ni}_{0.9}\text{Mn}_{0.05}\text{Co}_{0.05}\text{O}_2$.

Table S1. Fitting of impedance data of $\text{LiInSEB}^{\text{pNCM}}$ and $\text{LiInSEB}^{\text{sPPSLi/PVP-NCM}}$ at 25 °C using the transition line model.

$\text{LiInSEB}^{\text{pNCM}}$

Cycle number	1	2	52	102	152
$R_{\text{cathode}} / \Omega \text{ cm}^2$	18.5	34.7	124.2	150.5	203.4
$R_{\Omega} / \Omega \text{ cm}^2$	33.8	37.1	41.0	44.1	54.6
$R_{\text{anode}} / \Omega \text{ cm}^2$	6.8	1.5	15.7	27.3	37.7

$\text{LiInSEB}^{\text{sPPSLi/PVP-NCM}}$

Cycle number	1	2	52	102	152
$R_{\text{cathode}} / \Omega \text{ cm}^2$	26.4	35.2	69.7	90.3	110.4
$R_{\Omega} / \Omega \text{ cm}^2$	33.0	33.0	46.3	46.3	39.3
$R_{\text{anode}} / \Omega \text{ cm}^2$	2.9	1.8	26.6	25.7	31.4

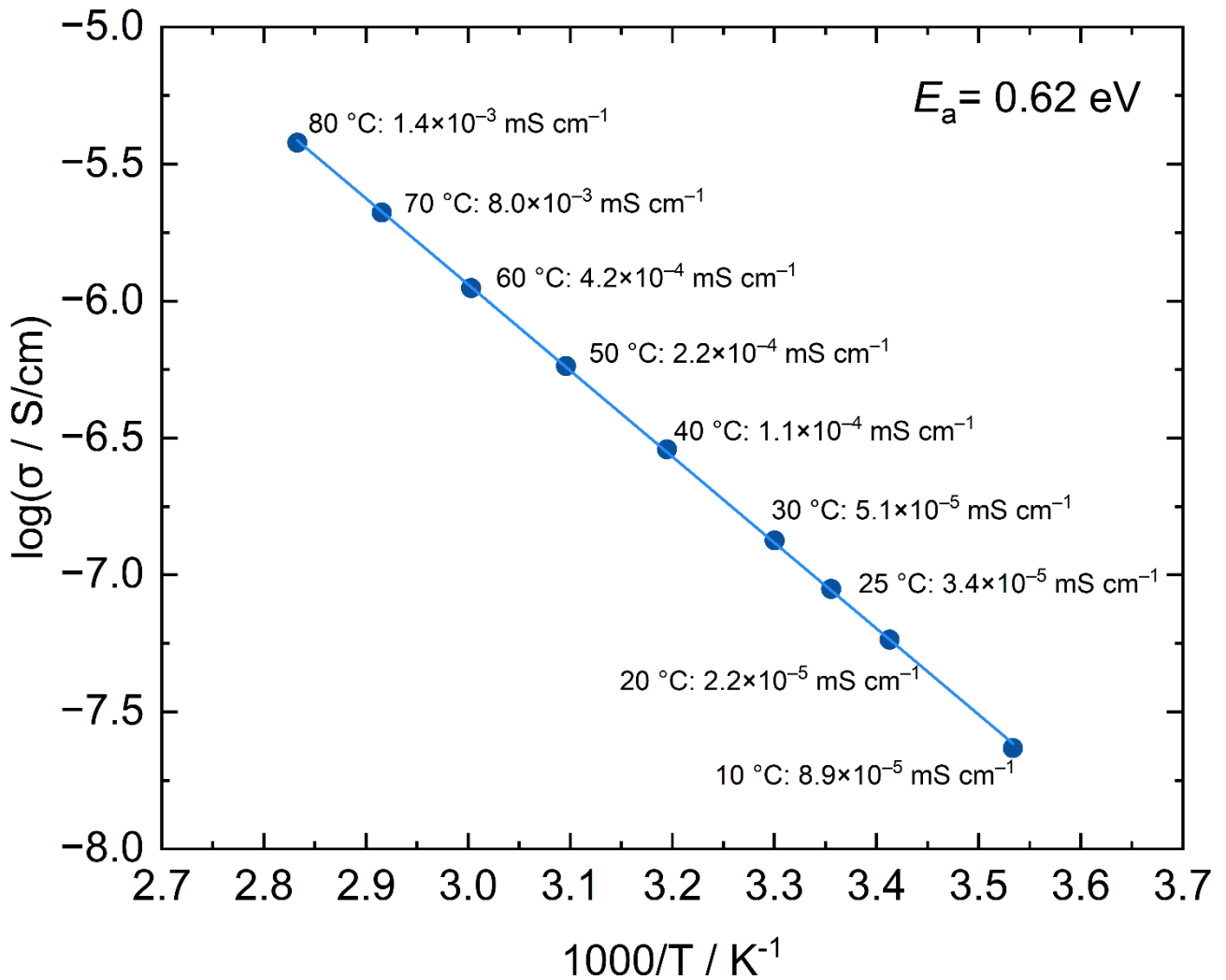


Figure S12. Arrhenius plot of conductivity of the sPPLi/PVP polymer complex obtained by compressing sPPLi/PVP into a pellet and applying a platinum sputter coating on both sides. The activation energy ($E_a = 0.62$ eV) is calculated by the slope of the $\log(\sigma / \text{S/cm})$ vs $1000/T / \text{K}^{-1}$, following the Arrhenius equation: $\sigma = \sigma_0 \cdot e^{-E_a/kT}$. σ is the conductivity measured by EIS. σ_0 is the pre-exponential factor. E_a is the activation energy. k is the Boltzmann constant $8.617 \cdot 10^{-5}$ eV/K. T is the temperature.